

## Solenoid elements in COSY INFINITY

**K. Makino<sup>†</sup> and M. Berz<sup>‡</sup>**

<sup>†</sup> Department of Physics, University of Illinois at Urbana-Champaign, 1110 W. Green Street, Urbana, IL 61801-3080, USA

<sup>‡</sup> Department of Physics and Astronomy, Michigan State University, East Lansing, MI 48824, USA

E-mail: makino@uiuc.edu, berz@msu.edu

**Abstract.** We describe a full array of solenoidal elements in the high order transfer map computation code COSY INFINITY, starting from a loop coil to any superposition of thick straight solenoids. Since the fringe field of coils extends very far longitudinally, and at the same time contains various nonlinearities due to the longitudinal dependence of the field, accurate but fast field computation is necessary. In COSY, the 3D fields along the integration of transfer map through such an element are computed using a Differential Algebra based PDE solver, which is very fast and only requires information about the analytical axial potential. By examples, we illustrate the feature of each solenoidal element and how to simulate realistic beamlines containing combinations of solenoids and other elements.

PACS numbers: 02.60.Cb, 02.60.Gf, 02.60.Lj, 05.45.-a, 29.27.-a, 29.27.Eg, 41.85.-p, 41.85.Ja, 41.85.Lc

### 1. Introduction

The differential algebraic (DA) methods [1, 2] allow the efficient computation and manipulation of high order Taylor transfer maps. When integrating transfer maps through electromagnetic fields, the full 3D fields are computed as part of each integration time step using DA PDE (partial differential equation) solvers. First, we address the mechanism of the method of DA fixed point PDE solvers, and as will be seen, the method is very compact and fast, and only requires the analytical axial potential for solenoidal elements.

After developing the theoretical background, we illustrate a variety of solenoidal elements available in COSY INFINITY [3], and study their features. Compared to multipole electromagnetic elements as dipoles, quadrupoles and so forth, the fringe fields of solenoids extend for a long distance. Particularly because of this long extension of the fringe fields, in practice it is important to be able to efficiently combine the fields consisting of several solenoidal coils, which are also treated with the DA PDE solvers. This often even simplifies the simulation efforts due to the shortened fringe fields created by the cancellation of fields of counteracting coils, as will be seen in an example from a muon beam cooling cell [4]. At last we show some examples of very atypical uses of standard electromagnetic elements, producing solenoidal fields from non-solenoidal elements, or producing bending fields from solenoidal elements. Such beam optical systems are particularly important in several components of neutrino factory designs [4].

## 2. DA fixed point PDE solvers

The idea of differential algebraic (DA) methods [1, 2, 5] is based on the observation that it is possible to extract more information about a function than its mere values on computers. One can introduce an operation  $T$  denoting the extraction of the Taylor coefficients of a pre-specified order  $n$  of the function  $f \in C^n(R^v)$ . In mathematical terms,  $T$  is an equivalence relation, and the application of  $T$  corresponds to the transition from the function  $f$  to the equivalence class  $[f]$  comprising all those functions with identical Taylor expansion in  $v$  variables to order  $n$ ; the classes are apparently characterized by the collection of Taylor coefficients. Since Taylor coefficients of order  $n$  for sums and products of functions as well as scalar products with reals can be computed from those of the summands and factors, the set of equivalence classes of functions can be endowed with well-defined operations, leading to the so-called Truncated Power Series Algebra (TPSA) [6, 7]. More advanced tools address the composition of functions, their inversion, solutions of implicit equations, and the introduction of common elementary functions[1]. For treatment of ODEs and PDEs, the power of TPSA can be enhanced by the introduction of derivations  $\partial$  and their inverses  $\partial^{-1}$ , corresponding to the differentiation and integration on the space of functions, resulting in the Differential Algebra  ${}_nD_v$ . This structure allows the direct treatment of many questions connected with differentiation and integration of functions, including the solution of the ODEs  $d\vec{x}/dt = \vec{f}(\vec{x}, t)$  describing the motion and PDEs describing the fields [5].

To any element  $[f] \in {}_nD_v$  we define the depth  $\lambda([f])$  as

$$\lambda([f]) = \begin{cases} \text{Order of first nonvanishing derivative of } f & \text{if } [f] \neq 0 \\ n+1 & \text{if } [f] = 0 \end{cases} .$$

In particular, any function  $f$  that does not vanish at the origin has  $\lambda([f]) = 0$ .

Let  $\mathcal{O}$  be an operator on the set  $M \subset {}_nD_v^m$ , where  ${}_nD_v^m$  is the set describing vector functions  $\vec{f} = (f_1, \dots, f_m)$  from  $R^v$  to  $R^m$ . Then we say that  $\mathcal{O}$  is contracting on  $M$  if for any  $\vec{a}, \vec{b} \in M$  with  $\vec{a} \neq \vec{b}$ ,

$$\lambda(\mathcal{O}(\vec{a}) - \mathcal{O}(\vec{b})) > \lambda(\vec{a} - \vec{b}).$$

In practical terms this means that after application of  $\mathcal{O}$ , the derivatives in  $\vec{a}$  and  $\vec{b}$  agree to a higher order than before application of  $\mathcal{O}$ . For example, the antiderivation  $\partial_k^{-1}$  is a contracting operator. Contracting operators satisfy a fixed point theorem:

**Theorem 1 (DA Fixed Point Theorem)** *Let  $\mathcal{O}$  be a contracting operator on  $M \subset {}_nD_v$  that maps  $M$  into  $M$ . Then  $\mathcal{O}$  has a unique fixed point  $a \in M$  that satisfies the fixed point problem  $a = \mathcal{O}(a)$ . Moreover, let  $a_0$  be any element in  $M$ . Then the sequence  $a_k = \mathcal{O}(a_{k-1})$  for  $k = 1, 2, \dots$  converges in finitely many steps (in fact, at most  $(n + 1)$  steps) to the fixed point  $a$ .*

The fixed point theorem is of great practical usefulness since it assures the existence of a solution, and moreover allows its exact determination in a very simple way in finitely many steps. The proof of the theorem can be found in [1]. The DA fixed point theorem has many useful applications, in particular a rather straightforward solution of ODEs and PDEs [5].

The direct availability of the derivation  $\partial$  and its inverse  $\partial^{-1}$  allows to devise efficient numerical PDE solvers of any order. The DA fixed point theorem allows one to solve PDEs iteratively in finitely many steps by rephrasing them in terms of a fixed point problem. The details depend on the PDE at hand, but the key idea is to eliminate differentiation with respect to one variable and replace it by integration. As an example, consider the rather general PDE

$$a_1 \frac{\partial}{\partial x} \left( a_2 \frac{\partial}{\partial x} V \right) + b_1 \frac{\partial}{\partial y} \left( b_2 \frac{\partial}{\partial y} V \right) + c_1 \frac{\partial}{\partial z} \left( c_2 \frac{\partial}{\partial z} V \right) = 0,$$

where  $a_1, a_2, b_1, b_2, c_1, c_2$  are functions of  $x, y, z$ . The PDE is re-written as

$$V = V|_{y=0} + \int_0^y \frac{1}{b_2} \left\{ \left( b_2 \frac{\partial V}{\partial y} \right) \Big|_{y=0} - \int_0^y \left[ \frac{a_1}{b_1} \frac{\partial}{\partial x} \left( a_2 \frac{\partial V}{\partial x} \right) + \frac{c_1}{b_1} \frac{\partial}{\partial z} \left( c_2 \frac{\partial V}{\partial z} \right) \right] dy \right\} dy.$$

The equation is now in fixed point form. Now assume the derivatives of  $V$  and  $\partial V/\partial y$  with respect to  $x$  and  $z$  are known in the plane  $y = 0$ . If the right hand side is contracting with respect to  $y$ , the various orders in  $y$  can be calculated by mere iteration.

As a particularly important example, consider the Laplace equation. It can be represented in general curvilinear coordinates [8, 9]. In the special case of a curvilinear coordinate system, the Laplace equation is obtained as [8, 9]

$$\Delta V = \frac{1}{1+hx} \frac{\partial}{\partial x} \left[ (1+hx) \frac{\partial V}{\partial x} \right] + \frac{\partial^2 V}{\partial y^2} + \frac{1}{1+hx} \frac{\partial}{\partial s} \left( \frac{1}{1+hx} \frac{\partial V}{\partial s} \right) = 0.$$

In the case of a straight section, where  $h = 0$ , it reduces to nothing but the Cartesian Laplace equation. The fixed point form of the Laplace equation in the planar curvilinear coordinates is

$$V = V|_{y=0} + \int_0^y \left( \frac{\partial V}{\partial y} \right) \Big|_{y=0} dy - \int_0^y \int_0^y \left\{ \frac{1}{1+hx} \frac{\partial}{\partial x} \left[ (1+hx) \frac{\partial V}{\partial x} \right] + \frac{1}{1+hx} \frac{\partial}{\partial s} \left( \frac{1}{1+hx} \frac{\partial V}{\partial s} \right) \right\} dy dy.$$

In this form, the right hand side has the interesting property that, regardless of what function  $V$  is inserted, the parts not depending on  $y$  are reproduced exactly, since all integrals introduce  $y$  dependence. Because of the integral operation, for a given choice of  $x$  and  $s$  and considering only the  $y$  dependence, the right hand side is contracting. In COSY INFINITY [3], the planar curvilinear Laplace equation is solved by the following very compact code

```
POLD := P ;
HF := 1+H*DA(IX) ;
HI := 1/HF ;
LOOP I 2 NOC+2 2 ;
  P := POLD - INTEG(IY, INTEG(IY,
    HI*( DER(IX, HF*DER(IX, P)) + DER(IS, HI*DER(IS, P)) ) ) ) ;
ENDLOOP ;
```

Here the boundary condition  $V|_{y=0} + \int_0^y (\partial V/\partial y)|_{y=0} dy$  is provided through the incoming form of  $P$ , which is obtained using the DA expression in COSY. The DA fixed point iteration converges to the solution potential  $P$  in finitely many steps.  $DA(IX)$  represents the identity for  $x$ ,  $NOC$  is the current transfer map computation order, and  $DER(I, \dots)$  and  $INTEG(I, \dots)$  correspond to the DA derivative and the DA anti-derivative operations with respect to the variable specified by the first argument  $I$ , namely “ $\partial_{x_I}$ ” and “ $\int_0^{x_I} dx_I$ ”. The full 3D field is derived from the solution potential  $P$ , using the elementary DA derivations  $\partial_x, \partial_y$  and  $\partial_s$ . In coded form, we have

```
BX := DER(IX, P) ;
BY := DER(IY, P) ;
BZ := DER(IS, P) ;
```

The advantages of the method are:

- Only the field in the midplane is needed
- The resulting field will always satisfy the stationary Maxwell equations

- The method works to any order

Another important coordinate system often suitable for computations under consideration are the cylindrical coordinates, in which the Laplace equation takes the simple form

$$\Delta V = \frac{1}{r} \frac{\partial}{\partial r} \left( r \frac{\partial V}{\partial r} \right) + \frac{1}{r^2} \frac{\partial^2 V}{\partial \phi^2} + \frac{\partial^2 V}{\partial s^2} = 0.$$

If  $V$  does not depend on  $\phi$ , namely  $V$  is rotationally symmetric, as in solenoid magnets, the fixed point form of the Laplace equation is simplified to

$$V = V|_{r=0} - \int_0^r \frac{1}{r} \int_0^r r \frac{\partial^2 V}{\partial s^2} dr dr,$$

and the right hand side is contracting with respect to  $r$ . Since we are only interested in cases in which  $V(s, r)$  is expressed in DA, if  $\partial^2 V / \partial s^2$  is nonzero, the integral  $\int_0^r r \partial^2 V / \partial s^2 dr$  contains  $r$  to a positive power. Thus, the factor  $1/r$  in the outer integral simply lowers the power of  $r$  by one, and the right hand side of the fixed point form can be evaluated in DA without posing trouble. To perform the DA fixed point iteration for the purpose of obtaining the full potential  $V(s, r)$ , one only needs to prepare the on-axis potential expression  $V(s, r)|_{r=0}$  as the boundary condition.

### 3. Single coil solenoid elements

We showed in the last section that for solenoid magnets, the DA PDE solver only requires an analytical expression of the potential on axis. In this section, we provide the on-axis field and potential of some solenoidal elements in the code COSY INFINITY [3] and discuss their features. In the following,  $R$  is the radius of the coil,  $R_1$  and  $R_2$  are the inner and outer radii of the coil if non-zero thickness is considered,  $I$  is the current,  $n$  is the number of turns per meter, and the coil extends from  $s = 0$  to  $s = l$ . While the on-axis forms are easily obtained, the out of axis forms can usually not be represented in closed form as they involve elliptic integrals; thus the ability of the DA PDE solver to generate the power series representation of the full 3D field to any order is very useful. Once the on-axis field  $B_z(s)$  is known, an on-axis potential  $V(s)$  can be determined via  $V(s) = \int B_z(s) ds$ . It is customary to omit the minus sign known for the electric case for magnetic scalar potential.

The first solenoid element is the current loop, consisting of a thin circular wire of radius  $R$  carrying the current  $I$ .

#### Current loop (COSY element CMR)

$$B_{z,\text{CMR}}(s) = \frac{\mu_0 I}{2R} \frac{1}{\left[1 + (s/R)^2\right]^{3/2}}, \quad V_{\text{CMR}}(s) = \frac{\mu_0 I}{2R} \frac{s}{\sqrt{1 + (s/R)^2}}.$$

The derivation of  $B_{z,\text{CMR}}(s)$  can be found in various text books on electromagnetism, for example, see eq. (5.40) (with  $\theta = 0$ ) in [10].

The next element is a thin coil extending from  $s = 0$  to  $s = l$ , made up of a single layer of thin wire carrying current  $I$  with  $n$  windings per meter.

#### Thin solenoid (COSY element CMSI)

$$B_{z,\text{CMSI}}(s) = \frac{\mu_0 I n}{2} \left( \frac{s}{\sqrt{s^2 + R^2}} - \frac{s-l}{\sqrt{(s-l)^2 + R^2}} \right),$$

$$V_{\text{CMSI}}(s) = \frac{\mu_0 I n}{2} \left( \sqrt{s^2 + R^2} - \sqrt{(s-l)^2 + R^2} \right).$$

$B_{z,\text{CMSI}}(s)$  can be obtained by integrating individual current loops positioned from  $s = 0$  to  $s = l$  as  $B_{z,\text{CMR}}(s) = n \cdot \int_0^l B_{z,\text{CMR}}(s-x)dx$ . Derivations of  $B_{z,\text{CMSI}}(s)$  can also be found in various text books, for example, see problem 5.2 in [10], where  $\cos \theta_1 = s/\sqrt{s^2 + R^2}$  and  $\cos \theta_2 = -(s-l)/\sqrt{(s-l)^2 + R^2}$  in our case. It is worth observing that in the middle, we have

$$B_{z,\text{CMSI}}(l/2) = \frac{\mu_0 In}{2} \cdot \frac{l}{\sqrt{(l/2)^2 + R^2}},$$

and if  $l \gg R$ , the field approaches the expected asymptotic value  $B_{z,\text{CMSI}}(l/2) \rightarrow \mu_0 In$ .

The next element is a thick coil extending longitudinally from  $s = 0$  to  $s = l$ , and radially from  $r = R_1$  to  $r = R_2$ , wound out of wire with a winding density  $n$  and carrying current  $I$ .

**Thick solenoid (COSY element CMST)**

$$B_{z,\text{CMST}}(s) = \frac{\mu_0 In}{2(R_2 - R_1)} \left[ s \log \left( \frac{R_2 + \sqrt{R_2^2 + s^2}}{R_1 + \sqrt{R_1^2 + s^2}} \right) - (s-l) \log \left( \frac{R_2 + \sqrt{R_2^2 + (s-l)^2}}{R_1 + \sqrt{R_1^2 + (s-l)^2}} \right) \right],$$

$$V_{\text{CMST}}(s) = \frac{\mu_0 In}{4(R_2 - R_1)} \left[ s^2 \log \left( \frac{R_2 + \sqrt{R_2^2 + s^2}}{R_1 + \sqrt{R_1^2 + s^2}} \right) - (s-l)^2 \log \left( \frac{R_2 + \sqrt{R_2^2 + (s-l)^2}}{R_1 + \sqrt{R_1^2 + (s-l)^2}} \right) \right. \\ \left. + R_2 \sqrt{R_2^2 + s^2} - R_1 \sqrt{R_1^2 + s^2} - R_2 \sqrt{R_2^2 + (s-l)^2} + R_1 \sqrt{R_1^2 + (s-l)^2} \right].$$

The derivation of the field for the thick solenoid is similar in spirit to the derivation of  $B_{z,\text{CMSI}}(s)$ . In fact, we have  $B_{z,\text{CMST}}(s) = 1/(R_2 - R_1) \cdot \int_{R_1}^{R_2} B_{z,\text{CMSI}}(s,R)dR$ . The factor  $1/(R_2 - R_1)$  is necessary to maintain the meaning of  $n$  as the number of windings per meter, i.e.  $In$  is the total current per meter. We observe that in the middle of the solenoid, we have

$$B_{z,\text{CMST}}(l/2) = \frac{\mu_0 In}{2(R_2 - R_1)} l \log \left( \frac{R_2 + \sqrt{R_2^2 + (l/2)^2}}{R_1 + \sqrt{R_1^2 + (l/2)^2}} \right).$$

If  $l \gg R_1, R_2$ , the log part in the right hand side of  $B_{z,\text{CMST}}(l/2)$  above is approximated as follows:

$$\log \left( \frac{R_2 + l/2}{R_1 + l/2} \right) \approx \log \left[ \left( 1 + \frac{2R_2}{l} \right) \left( 1 - \frac{2R_1}{l} \right) \right] \approx \log \left[ 1 + \frac{2}{l} (R_2 - R_1) \right] \approx \frac{2}{l} (R_2 - R_1).$$

So the field approaches the asymptotic value  $B_{z,\text{CMST}}(l/2) \rightarrow \mu_0 In$ .

Traditionally, also various other approximate representations of fields have been used (see for example [11, 12, 13, 14]) that are based on particularly simple forms for the fields or potentials; of these approximations, we have implemented two. One of them is the Glaser lens, which is frequently used to approximately describe a lens made of a coil with finite but short length and finite but small thickness.

**Glaser lens (COSY element CML)**

$$B_{z,\text{CML}}(s) = \frac{B_0}{1 + (s/R)^2}, \quad V_{\text{CML}}(s) = B_0 R \arctan(s/R).$$

The other frequently used approximation is for an extended coil of length  $l$  of small thickness of the form.

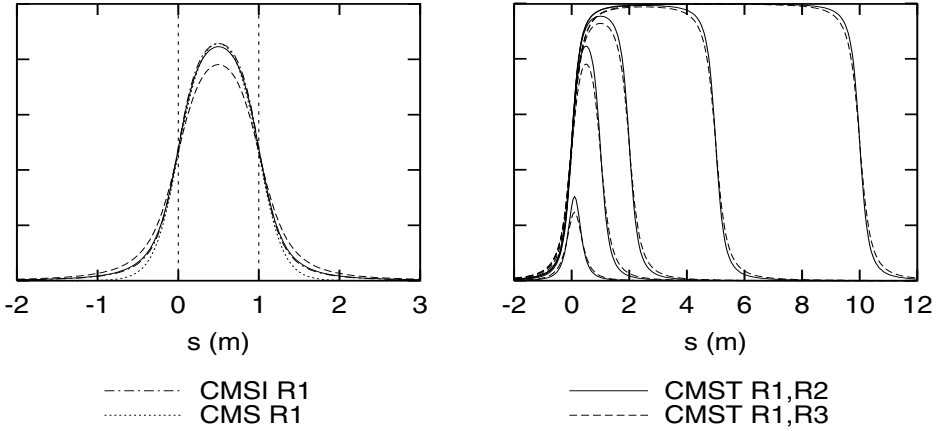


**Figure 1.** The axial field profile  $B_z(s)$  of various COSY solenoid elements. Left: Comparison between the thin element CMSI, the tanh approximation element CMS, and the thick element CMST. The length is  $l = 1\text{m}$ . Right: Comparison of different lengths  $l = 0.3\text{m}$ ,  $1\text{m}$ ,  $2\text{m}$ ,  $5\text{m}$  and  $10\text{m}$  for CMST. The (inner) radius is  $R_1 = 0.3\text{m}$ . For CMST, the outer radii  $R_2 = 0.33\text{m}$  and  $R_3 = 0.5\text{m}$  are compared. The field strength is scaled relative to the asymptotic value  $\mu_0 I n$ .

### Thin solenoid (tanh approximation) (COSY element CMS)

$$B_{z,\text{CMS}}(s) = \frac{B_0}{2 \tanh(l/2R)} [\tanh(s/R) - \tanh((s-l)/R)], \quad B_{z,\text{CMS}}(l/2) = B_0.$$

$$V_{\text{CMS}}(s) = \frac{B_0}{2 \tanh(l/2R)} R [\log(\cosh(s/R)) - \log(\cosh((s-l)/R))].$$

Here the hyperbolic tangents are used as simple approximations for the rise and fall-off of the field at  $s = 0$  and  $s = l$ , respectively.

As the analytical expressions of the on-axis field  $B_z(s)$  and the potential  $V(s)$  indicate, the profiles of  $s$ -dependence are characterized by the ratio of the length  $l$  and the aperture  $R$ . Figure 1 shows the axial field profile  $B_z(s)$  of the elements CMSI, CMS, and CMST of length  $l = 1\text{m}$  with the radius  $R_1 = 0.3\text{m}$  and the outer radius  $R_2 = 0.33\text{m}$  or  $R_3 = 0.5\text{m}$  (Left), and the field profile of CMST of different lengths  $l = 0.3\text{m}$ ,  $1\text{m}$ ,  $2\text{m}$ ,  $5\text{m}$  and  $10\text{m}$  (Right). The field strength is scaled relative to the asymptotic value  $\mu_0 I n$ , and  $B_0$  for CMS is given by  $B_{z,\text{CMSI}}(l/2)$ . As the length study picture shows, many realistic solenoids do not even reach maximum fields close to the asymptotic value  $\mu_0 I n$ .

The tanh approximation as in the element CMS is commonly used because the on-axis field drops more swiftly in the fringe region compared to the pure theoretical fields as CMSI and CMST, which simplifies the simulation effort. On the other hand, the discrepancy from the actual field becomes very large particularly for sufficiently thick solenoids, which are important in practice because of their ability to provide high field strength. Figure 2 shows the full 3D field distributions  $B_z(s, r)$  and  $B_r(s, r)$  of the thick element CMST of length  $l = 1\text{m}$  with the radii  $R_1 = 0.3\text{m}$  and  $R_2 = 0.33\text{m}$ . The full 3D field is derived only from the on-axis potential  $V(s)$  via the DA fixed point PDE solver.

Some matrix elements of fifth order transfer maps of these solenoid elements are listed below in COSY notation for comparison, showing the differences in the linear and nonlinear behavior. Similar to before, the length is  $l = 1\text{m}$ , the (inner) radius is  $R = R_1 = 0.3\text{m}$ , and the

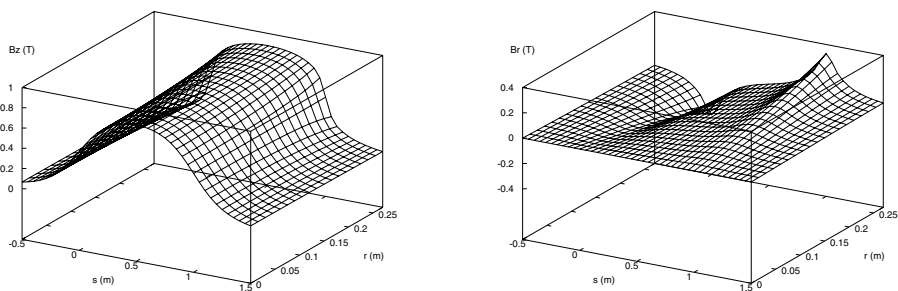


**Figure 2.** The full 3D field distributions  $B_z(s, r)$  (Left) and  $B_r(s, r)$  (Right) of the thick element CMST ( $l=1\text{m}$ ,  $R_1=0.3\text{m}$ ,  $R_2=0.33\text{m}$ ) derived only from the on-axis potential  $V(s) = \int_s B_z(s)$  using the DA fixed point PDE solver. The field strength is scaled relative to the asymptotic value  $\mu_0 I n$ .

outer radii used in CMST are  $R_2=0.33\text{m}$  and  $R_3=0.5\text{m}$ . The magnet strength is adjusted to have  $\mu_0 I n = 1\text{Tesla}$ , and  $B_0$  for CMS is scaled to agree with  $B_{z,\text{CMST}}(l/2)$ .

CMST1:

x_f	a_f	y_f	b_f	xayb
0.7937713	-0.1431056	-0.4573031	0.8243452E-01	1000
0.8436961	0.7938225	-0.4860026	-0.4572141	0100
...	...	...	...	....
-0.4911018E-01	-0.4490695	-0.3866000	-0.8418896	0014
0.2409343	-0.6962362E-01	0.1265599	-0.2574890	0005

CMS:

0.8152097	-0.1403695	-0.4257566	0.7331028E-01	1000
0.8629072	0.8152097	-0.4506673	-0.4257566	0100
...	...	...	...	....
-0.2386703E-01	-0.3563119	-0.3615158	-0.7512712	0014
0.2331341	-0.5329836E-01	0.1522912	-0.2406150	0005

CMST with R1, R2:

0.7953672	-0.1399478	-0.4582230	0.8061561E-01	1000
0.8446078	0.7954184	-0.4865284	-0.4581341	0100
...	...	...	...	....
-0.4865521E-01	-0.3911095	-0.3711714	-0.7356460	0014
0.2426523	-0.5600330E-01	0.1324498	-0.2326217	0005

CMST with R1, R3:

0.8034393	-0.1239508	-0.4628757	0.7140094E-01	1000
0.8494714	0.8034915	-0.4893318	-0.4627851	0100
...	...	...	...	....
-0.4406906E-01	-0.2077903	-0.3039852	-0.3947231	0014
0.2456954	-0.1146626E-01	0.1444507	-0.1507266	0005

The thinner case of CMST with  $R_1$  and  $R_2$  agrees with the map of CMSI to approximately two digits. On the other hand, the map of CMS agrees with that of CMSI to approximately only one digit. This again shows that the tanh approximation element CMS has to be used with care.

#### 4. Multiple coil solenoids

If a system consists of several solenoids, it is often crucial to be able to treat the whole solenoidal system as one element with superimposed solenoidal field, because the fringe field extension is particularly long for solenoids. In this section, we present such an example from muon beam ionization cooling systems. The example is a 2.75m sFOFO muon beam ionization cooling cell in Muon Feasibility Study II [4]. There are three coils in the cell, and the starting position of each coil is 0.175m, 1.21m, and 2.408m. The outer two coils are 0.167m long with the inner and outer radii 0.33m and 0.505m and the current density is  $75.2\text{A}/\text{mm}^2$ . The middle one is 0.33m long with the radii 0.77m and 0.85m and the current density  $98.25\text{A}/\text{mm}^2$  [4]. The pictures in Figure 3 show the coil layout and the superimposed axial field profile  $B_z(s)$  as well as the full 3D field distributions of  $B_z(s, r)$  and  $B_r(s, r)$  that

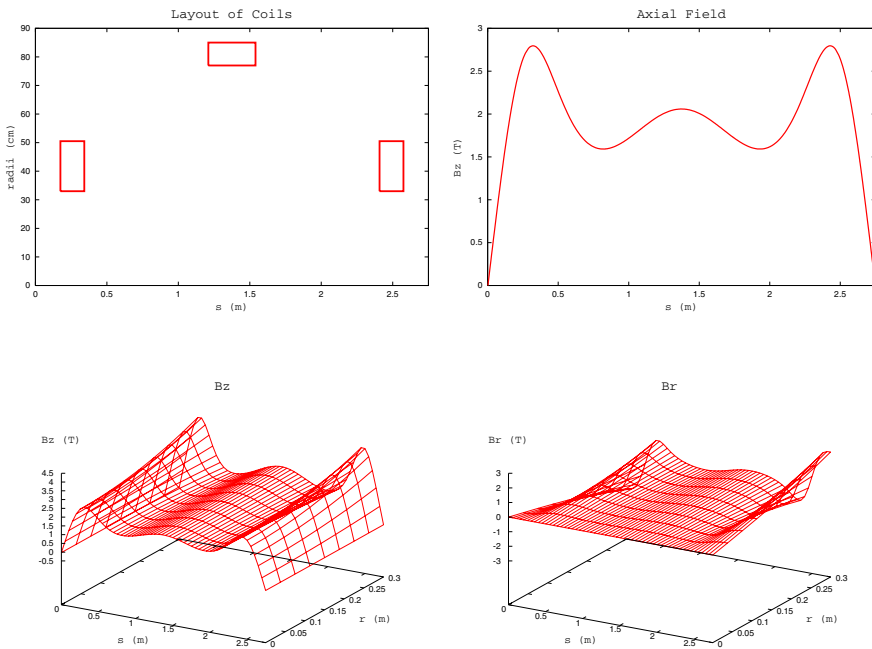


**Figure 3.** The coil layout, the superimposed axial field profile  $B_z(s)$ , and the full 3D field distributions of  $B_z(s, r)$  and  $B_r(s, r)$  of a 2.75m sFOFO cell [4].  $B_z(s, r)$  and  $B_r(s, r)$  are derived only from the on-axis potential using the DA fixed point PDE solver.

are obtained via the DA fixed point PDE solver. Since the thickness of coils is very large, the superimposed field maintains high strength throughout the cell except for the ends of the cell, where the axial field drops to zero due to the alternating field direction in the preceding and following cells. In fact, the drop of the axial field to zero simplifies the computation of high order transfer maps by beginning and ending the computation at a zero crossing of the field, although of course the original reason for the design need for field flips is to enhance cooling efficiency [4].

The muon beam cooling cell has accelerating cavities and absorbers situated inside the solenoids. We can treat such systems with the transfer map in a split operator framework approach by slicing the cell into short pieces so that the effects of each element can be superimposed by inserting a short negative drift [5]. For example, the 2.75m sFOFO cell is sliced into about 80 pieces [5].

## 5. Vertical solenoidal fields and misalignment

The modern concept of designing beam optical systems is to perform each of the common tasks of bending, focusing, and nonlinear correction by separate elements; but there are situations in which this simple concept would lead to significant sacrifices. For example, the beam optical systems for rare and short-lived particles often require complicated setups including combined function electromagnetic elements to manipulate the beam efficiently, an example of which has been provided above. Sometimes misalignment by displacement and tilts of regular kind of single function elements can achieve the necessary combined fields. The complication brought by the misalignment has to be studied carefully, because sometimes it may lead to unexpected beam dynamics.

We show an example using a design of the  $60^\circ$  arc cell of a compact muon storage ring [4]. The cell was designed to achieve a very high degree of compactness using half overlapping coils as shown in Figure 4. The double layered part has a strong dipole field of 7 Tesla, and the single layered part has a dipole field component of around half that strength. In addition, the latter region exhibits a skew quadrupole field which is used for focusing purposes, as well as small high order multipole components introduced mostly because of the limited horizontal width of the coils. The longitudinal magnet layout produces a longitudinal field component, breaking midplane symmetry, and the on-axis longitudinal field, in other words the solenoidal field, is as strong as 2.2 Tesla; Figure 4 shows the strength as a function

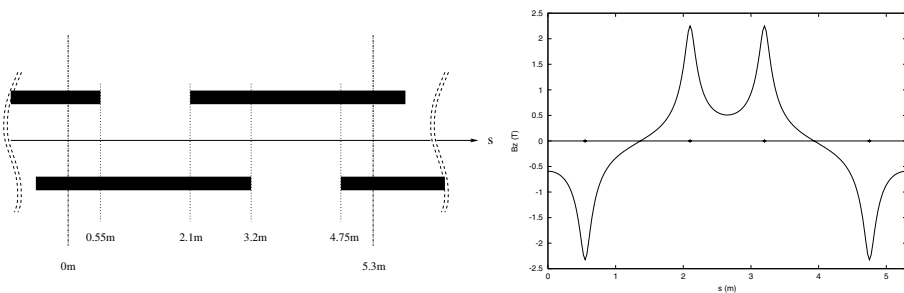


**Figure 4.** The longitudinal magnet layout (Left) and the on-axis field profile of solenoidal field component  $B_z(s)$  (Right) of a design of the  $60^\circ$  arc cell of a compact muon storage ring [4].

of position  $s$ . By using the technique discussed in the previous section for superimposed solenoidal fields, the effects of the solenoidal field of the  $60^\circ$  arc cell can be included in the beam dynamics study.

Due to limitations of space, we refrain from providing details about the results of simulations of the resulting particle dynamics; various such results are given in [4].

Another interesting example of misalignment is a design of a muon beam cooling ring using short solenoids with large aperture [15] that are tilted horizontally to deflect the reference orbit of the beam and overall lead to the possibility of operating without dipoles [16]. Utilizing the COSY commands for misalignment, it is also possible to analyze such bending beamlines consisting of only solenoidal elements.

## Acknowledgments

The work was supported by the Illinois Consortium for Accelerator Research, the US Department of Energy, an Alfred P. Sloan Fellowship and the National Science Foundation.

## References

- [1] M. Berz. *Modern Map Methods in Particle Beam Physics*. Academic Press, San Diego, 1999.
- [2] M. Berz. Differential algebraic description of beam dynamics to very high orders. *Particle Accelerators*, 24:109, 1989.
- [3] M. Berz and K. Makino. COSY INFINITY Version 8.1 - user's guide and reference manual. Technical Report MSUHEP-20704, Department of Physics and Astronomy, Michigan State University, East Lansing, MI 48824, 2001. See also <http://cosy.pa.msu.edu>.
- [4] S. Ozaki et al. for the Muon Collaboration. Feasibility study-II of a muon-based neutrino source. Technical Report 52623, Muon Collider Collaboration, BNL, 2001.
- [5] K. Makino, M. Berz, D. Errede, and C. J. Johnstone. High order map treatment of superimposed cavities, absorbers, and magnetic multipole and solenoid fields. *Nuclear Instruments and Methods*, in print, 2003.
- [6] M. Berz. The new method of TPSA algebra for the description of beam dynamics to high orders. Technical Report AT-6:ATN-86-16, Los Alamos National Laboratory, 1986.
- [7] M. Berz. The method of power series tracking for the mathematical description of beam dynamics. *Nuclear Instruments and Methods*, A258:431, 1987.
- [8] K. Makino. *Rigorous Analysis of Nonlinear Motion in Particle Accelerators*. PhD thesis, Michigan State University, East Lansing, Michigan, USA, 1998. Also MSUCL-1093.
- [9] K. Makino and M. Berz. Perturbative equations of motion and differential operators in nonplanar curvilinear coordinates. *International Journal of Applied Mathematics*, 3,4:421–440, 2000.
- [10] J. D. Jackson. *Classical Electrodynamics*. Wiley, New York, 1975.
- [11] W. Glaser. *Grundlagen der Elektronenoptik*. Springer, Wien, 1952.
- [12] X. Jiye. *Aberration Theory in Electron and Ion Optics*. Advances in Electronics and Electron Physics, Supplement 17. Academic Press, Orlando, Florida, 1986.
- [13] P. W. Hawkes and E. Kasper. *Principles of Electron Optics*, volume 1-2. Academic Press, London, 1989.
- [14] K. G. Steffen. *High Energy Beam Optics*. Wiley-Interscience, New York, 1965.
- [15] J. S. Berg, R. C. Fernow, and R. B. Palmer. An alternating solenoid focused ionization cooling ring. The Muon Collider and Neutrino Factory Notes MUC-NOTE-COOL-THEORY-0239, Fermi National Accelerator Laboratory, 2002. See <http://www-mucool.fnal.gov/notes/notes.html>.
- [16] J. S. Berg, R. C. Fernow, and R. B. Palmer. Private communication, 2002.